Delft University of Technology

Stability Enhanced Design of EV Chargers for Weak Grid Connection

Wang, Lu; Qin, Zian; Wu, Yang; Bauer, Pavol

Stability Enhanced Design of EV Chargers for Weak Grid Connection

1ˢᵗ Lu Wang
Electr. Sustainable Energy
TU Delft
Delft, The Netherlands
l.wang-11@tudelft.nl

2ⁿᵈ Zian Qin
Electr. Sustainable Energy
TU Delft
Delft, The Netherlands
z.qin-2@tudelft.nl

3ʳᵈ Yang Wu
Electr. Sustainable Energy
TU Delft
Delft, The Netherlands
y.wu-6@tudelft.nl

4ᵗʰ Pavol Bauer
Electr. Sustainable Energy
TU Delft
Delft, The Netherlands
p.bauer@tudelft.nl

Abstract—**Reinforcement of the legacy grid infrastructure will be very costly and thereby unrealistic. Consequently, weak grid connection of electric vehicle (EV) chargers will sooner or later be the case. It may however bring instability issues since the EV chargers that can work well in strong grid conditions usually do not fit the weak grid conditions. Aiming at design guidelines, this digest analyzes the influence of the charger's design on the stability of the grid connection. Simulations and experiments are carried out to verify the analysis results.**

Index Terms—**EV Charging, Small-signal Stability, Controller Design, Impedance Based Method**

I. INTRODUCTION

Amid the widespread adoption of electric vehicles (EVs), these years witness a dramatic increase of charging infrastructures. To provide satisfactory experience for individuals, the charging service should be easily accessible and reliable [1], [2]. However, EV chargers, essentially power-electronic-based devices, might have the small-signal instability issue and are fragile to cyber-attacks [3] due to the increasing use of internet-of-things (IoT) technology, e.g. OCPP-compliant chargers.

To study small-signal instability induced by the interaction between the grid and the charger, a promising approach is the impedance based method [4]–[7]. Through the impedance based approach, it is revealed that small-signal instability is more prone to happen if a charger is connected to a weak grid [8]. However, connecting a charger to a weak grid is very likely to happen. For instance, due to the highly impulsive charging power profile of an EV [1], it is reasonable to install a battery storage system in an EV charging station to supply the peak charging power. In this way, it reduces the costs of upgrading the grid infrastructures but leads to a smaller grid capacity and a weak grid condition for the charger. Thus, if the charger's front-end converter, i.e., the rectifier, is not properly designed, instability may appear.

Previous studies [9], [10] show that using a higher bandwidth of the current loop (CL) and a smaller bandwidth the

voltage loop (VL) is beneficial for keeping stability of a rectifier with a weak grid connection. It is a simple guideline for the controller design. However, as revealed later in this paper, increasing the VL bandwidth and CL bandwidth does not necessarily reduce the stability margin and make the system tend to be unstable. The reason is that the bandwidth has an indirectly influence on the impedance, which is established based on the influence of the cutoff frequency and the damping ratio of the control loop on the input impedance. To support this statement, detail study is presented later.

Besides, many fast EV chargers have a modular design [1], [11], meaning a charger consists of several power modules to scale down the power rating of each. The power module will have a different design of the controller and the power filter compared with a one-unit design, due to its lower power rating. The impact of using a modular design on stability however has rarely been studied.

Aiming at stability enhanced design of the EV charger with a weak grid connection, this digest gives a comprehensive study on the influence of the control loops, namely VL and CL, on the input impedance and eventually the stability. The influence of the PLL, however, is not discussed because PLL design dominant the stability of an inverter but not a rectifier [12]. Additionally, on top of the study on the influence of the control loops on the impedance, the paper studies the impact of choosing a modular design on the small-signal stability.

The rest of the paper is organized as follows. Section II introduces the small-signal stability criteria and the studied system that is typically used for an EV charger's front end converter. Section III is devoted to the influence of the control loop design and the power filter inductance on the input impedance. In Section IV, the input impedance of a charger with a modular design and the one with a one-unit design is compared, which reveals that using a modular design tends to decrease the stability margin of a charging system. Finally, the paper concludes in Section V.

II. SYSTEM DESCRIPTION AND STABILITY CRITERIA

The three-phase active front end (AFE) shown in Fig. 1 is considered for analysis. More specifically, the 2-level AFE is considered in the study because it is a typical topology for EV charger rectifiers [13], [14]. Further, as one of the typical

control methods, three proportional-integral (PI) controller are considered for the PLL, the alternating current control (ACC), and the DC-link voltage control (DVC), respectively.
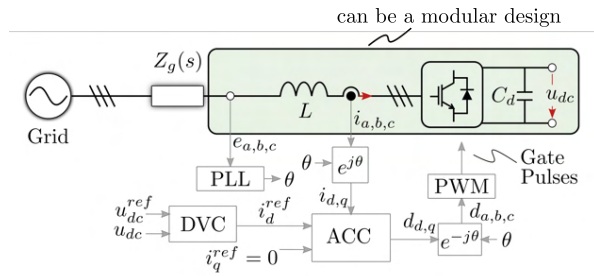
Fig. 1. Typical system configuration of the three-phase AFE of an EV charger.
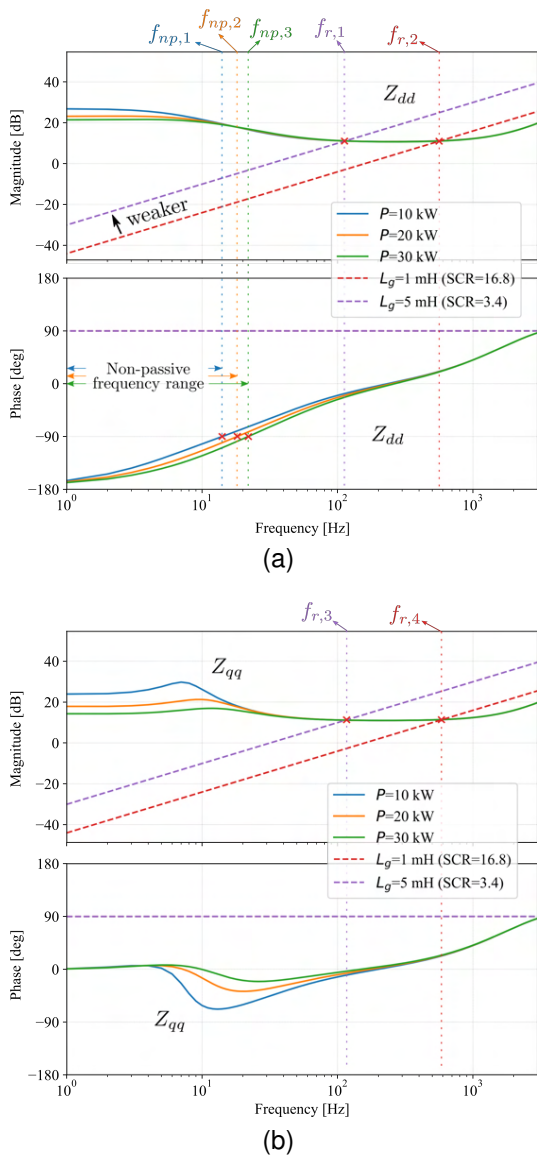
Fig. 2. Bode plots of the (a) $Z_{dd}(s)$ and the $Z_{qq}(s)$ at three charging powers.

The input impedance of an AFE in the synchronous dq-frame is a two-by-two matrix $\mathbf{Z_{AFE}}(s)$ whose diagonal elements are $Z_{dd}(s)$ and $Z_{qq}(s)$. The off-diagonal elements of $\mathbf{Z_{AFE}}(s)$ are coupling impedance, namely $Z_{dq}(s)$ and $Z_{qd}(s)$. The magnitude of the coupling impedance is much smaller than the diagonal impedance when the power factor of the AFE is unity. In this case, the stability is dominated by the diagonal impedances [15], [16] and can be analyzed by the passivity stability criteria [9]. Specifically, a 30-kW AFE's input impedance is extracted based on the modeling in [17], [18]. The bode plots of the $Z_{dd}(s)$ and the $Z_{qq}(s)$ of the AFE at three charging powers are shown in Fig. 2. As seen, $Z_{dd}(s)$ is non-passive at low frequencies where its phase is lower than $-90°$ or higher than $90°$, which is caused by the current control, PLL, and voltage control together. Further, the non-passive frequency range of $Z_{dd}(s)$ is wider if the charging power is higher. As for $Z_{qq}(s)$, it is passive at all frequencies of interest because the AFE is in the rectifier mode. When the grid is weaker and the short circuit ratio (SCR) is lower, the two resonant frequencies $f_{r,2}$ and $f_{r,4}$ decreases to $f_{r,1}$ and $f_{r,3}$, respectively. If the grid becomes even weaker so that the resonant frequency is within the non-passive frequency range, the grid-charger system will become unstable.

Apparently, if the non-passive frequency range of the $Z_{dd}(s)$ is smaller and the magnitude $|Z_{dd}(s)|$ is bigger, the grid-charger system can stay stable for a broader set of grid impedance values.

III. INFLUENCE OF CONTROLLER DESIGN ON THE INPUT IMPEDANCE

A. Requirements on the control loop responses

Practically, the controller parameters should be properly tuned to achieve a desired control response that is generally specified with phase margin, gain margin, damping ratio, cut-off frequency, bandwidth and etc. Satisfying these requirements ensure a stable and fast control response. Thus, how these control loop specifications, instead of the controller parameters, influence the input impedance will be discussed.

With dq-axis decoupling, the d-axis current loop can be simplified as Fig. 3. The parameter L is the inductance of the power filter. Based on the simplified model, the damping ratio and the cut-off frequency can be approximated as

$$\omega_{c,CL} = \frac{k_{pi}}{L}, \quad \delta_{CL} = \frac{1}{2}\sqrt{\frac{k_{pi}^2}{L \cdot k_{ii}}} \quad (1)$$

As a result, the bandwidth of the current loop can be approximated as

$$\omega_{b,CL} = \omega_{ni} \cdot \sqrt{1 + 2 \cdot \delta_{CL}^2 + \sqrt{(2 \cdot \delta_{CL}^2 + 1)^2 + 1}} \quad (2)$$

where

$$\omega_{ni} = \frac{\omega_{c,CL}}{2 \cdot \delta_{CL}}.$$

The block diagram of the voltage loop is shown in Fig. 4. E_d and U_{dc} denote the grid voltage amplitude and the DC-link voltage, respectively. $G_{c,cl}(s)$ denotes the close loop transfer
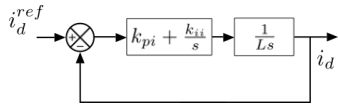
Fig. 3. Block diagram of the d-axis current loop.

function of the current loop. Typically, the inner current loop should have much higher bandwidth than the outer voltage loop and the PLL. Therefore, $G_{c,cl}(s)$ can be approximated as 1 when analyzing the loop response of the much slower voltage loop. Consequently, the damping ratio and the cut-off frequency can be approximated as

$$\omega_{c,VL} = \frac{3 \cdot E_d \cdot k_{pu}}{2 \cdot U_{dc} \cdot C_d \cdot s}, \quad \delta_{VL} = \frac{1}{2}\sqrt{\frac{3 \cdot E_d \cdot k_{pu}^2}{2 \cdot U_{dc} \cdot C_d \cdot k_{iu}}} \quad (3)$$

As a result, the bandwidth of the voltage loop can be
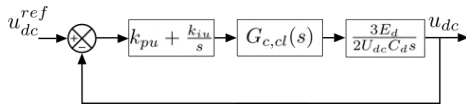
Fig. 4. Block diagram of the voltage loop.

approximated as

$$\omega_{b,VL} = \omega_{nv} \cdot \sqrt{1 + 2 \cdot \delta_{VL}^2 + \sqrt{(2 \cdot \delta_{VL}^2 + 1)^2 + 1}} \quad (4)$$

where

$$\omega_{nv} = \frac{\omega_{c,VL}}{2 \cdot \delta_{VL}}.$$

Typically, the damping ratio should be larger than 0.7 to obtain enough phase margin and an acceptable overshoot, e.g., 10%. However, the damping ratio should not be too small otherwise the loop response is too sluggish. Besides, the current loop bandwidth should be below one-tenth of the switching frequency to attenuate the switching noises.

Since the controller is tuned to satisfy these loop response requirements, directly analyzing the influence of these control loop specifications on the input impedance is more worthwhile than analyzing the controller parameters' influence on the input impedance.

B. Influences of the control loop specifications on the input impedance

The analysis in Section II reveals that increasing the magnitude $|Z_{dd}(s)|$ and narrowing the non-passive frequency range of $Z_{dd}(s)$ is beneficial for maintaining the stability of a grid-charger system in a weak grid condition.

Fig. 5 shows the influence of the VL damping ratio on the $Z_{dd}(s)$. As seen, a higher VL damping ratio not only increases the $|Z_{dd}(s)|$ but also narrows the non-passive frequency range. Thus, a higher VL damping ratio is preferred to maintain stability when connecting the chargers to weak grids.

The effect of the CL damping ratio δ_{CL} is different than the effect of δ_{VL}. Fig. 6 shows that increasing δ_{CL} can effectively narrow the non-passive region. However, a higher δ_{CL} also
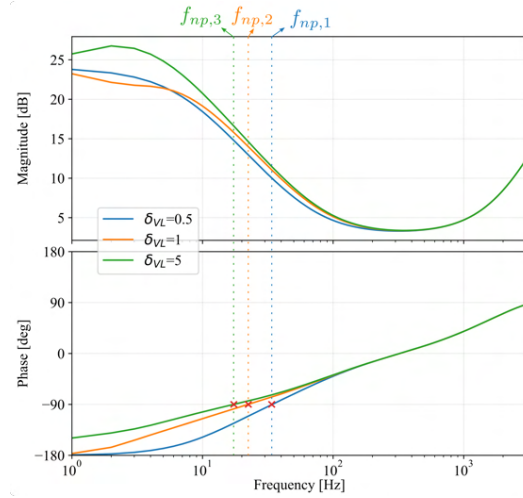
Fig. 5. Bode plots of the $Z_{dd}(s)$ with three different VL damping ratio.

brings a lower magnitude of $Z_{dd}(s)$ at low frequencies, which leads to a lower resonant frequency. Nevertheless, when the damping ratio is enough high, continually increasing δ_{CL} does not effectively decrease $|Z_{dd}(s)|$ but significantly reduces the non-passive region. Therefore, when designing a charger to be connected to a weak grid, a high δ_{CL} is still preferred to effective shrink the non-passive region. The magnitude $|Z_{dd}(s)|$ can be increased, as revealed later, by increasing $\omega_{c,CL}$.
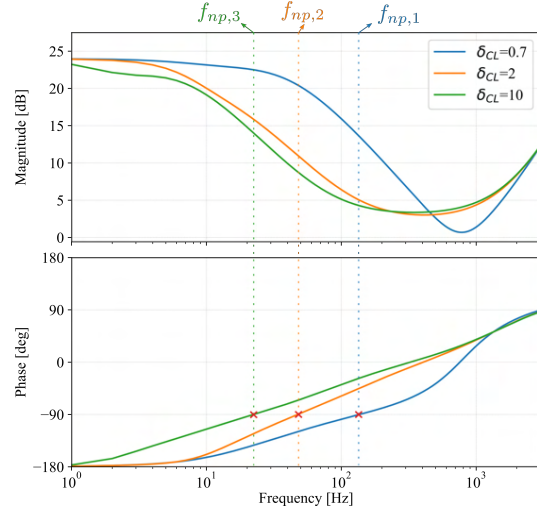
Fig. 6. Bode plots of the $Z_{dd}(s)$ with three different CL damping ratio.

Except for the damping ratio, the cut-off frequency of the current loop and the voltage loop also have significant influence on the input impedance. Fig. 7 shows the influence of $\omega_{c,CL}$ on $Z_{dd}(s)$. Clearly, a higher $\omega_{c,CL}$ leads to a significant higher $|Z_{dd}(s)|$ but a slightly wider non-passive region. Thus, a higher $\omega_{c,CL}$ is preferred in a weak grid connection situation.

1233
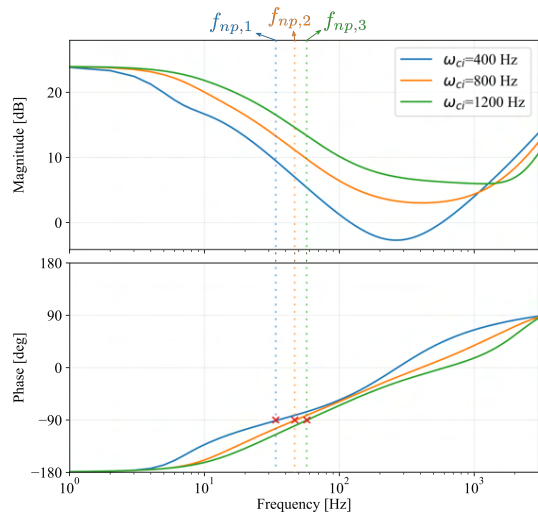
Fig. 7. Bode plots of the $Z_{dd}(s)$ with three different $\omega_{c,CL}$.

Fig. 8 reveals the influence of $\omega_{c,VL}$ on $Z_{dd}(s)$. With the increase of $\omega_{c,VL}$, the non-passive region is clearly broader whereas $|Z_{dd}(s)|$ almost remains the same. Therefore, a small $\omega_{c,VL}$ is preferred to ensure the charger properly operates with a weak grid connection.
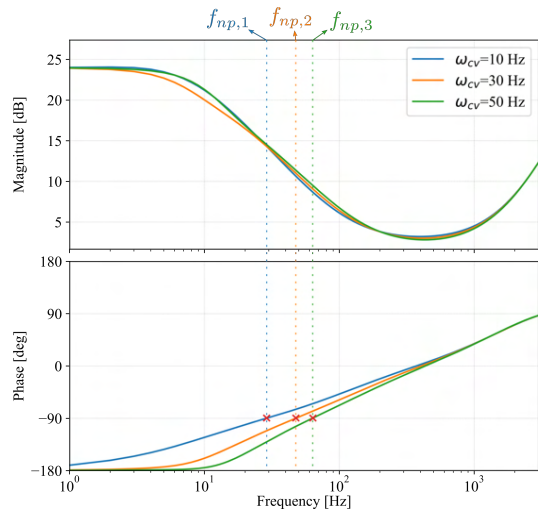
Fig. 8. Bode plots of the $Z_{dd}(s)$ with three different $\omega_{c,VL}$.

It is worth mentioning that a higher bandwidth of the current loop and voltage loop does not necessarily reduce the stability margin of the charging system. For example, Fig. 9 compares the stability of two chargers with different current loop designs. Design 1 has a higher CL bandwidth, i.e., 850 Hz, whereas Design 2 has a lower CL bandwidth, i.e., 650 Hz. Clearly, the resonant frequency $f_{r,1}$ is larger than $f_{np,1}$ indicating Design 1 is stable when SCR is 3.4. However, it is seen that the charger with Design 2 is unstable when SCR is 3.4 because the resonant frequency $f_{r,2}$ locates inside the non-passive region. Therefore, the influence of the CL bandwidth

on the stability of the charging system is indirect and may change from one case to another.
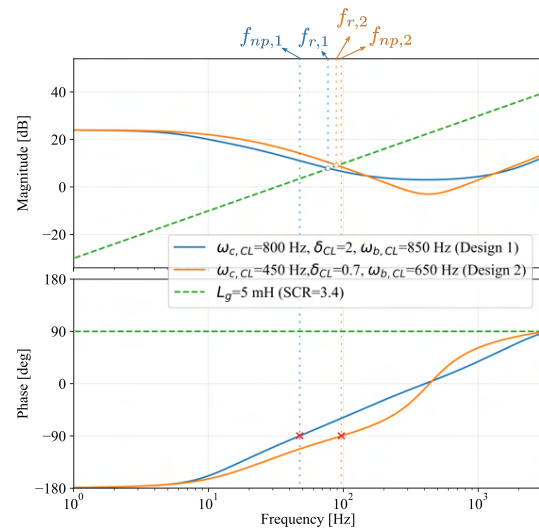
Fig. 9. Bode plots of the $Z_{dd}(s)$ with three different $\omega_{b,CL}$.

C. Influence of the power filter inductance on the input impedance

Except from the controller parameters, the inductance of the power filter also significantly influence the stability of the charging system. The input impedance of three chargers with different filter inductance are compared in Fig. 10. Accordingly, it is noticed that the inductance only influence $|Z_{dd}(s)|$. Specifically, increasing the power filter inductance can increase $|Z_{dd}(s)|$ leading to a larger stability margin if the other parameters are not changed. Consequently, a large filter inductance is preferred from the small-signal stability perspective.
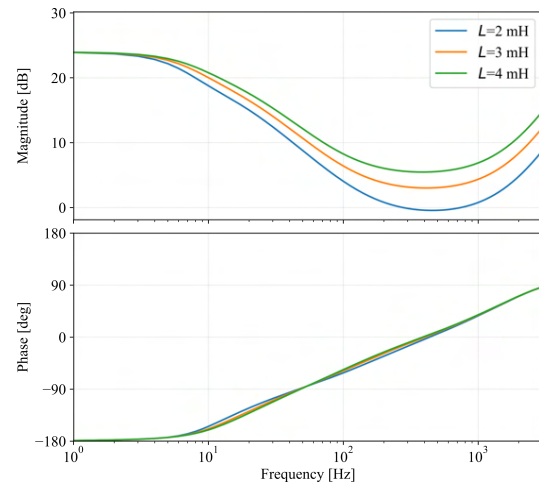
Fig. 10. Bode plots of the $Z_{dd}(s)$ with three different power filter inductance L.

It is worth mentioning that when comparing the input impedance of the charger with different filter inductance, the

1234

cutoff frequency of the current loop should be kept the same. Otherwise, the difference among the three designs does not purely stem from the change of the inductance.

IV. MODULAR DESIGN VS ONE-UNIT DESIGN

In a modular design based charger, each power module has a smaller power rating than the charger's nominal power. Consequently, the switching frequency of the AFE in each power module can be higher than the charger using a one-unit design. As the result, it is common that a modular design based AFE has higher CL bandwidth, higher VL bandwidth, and smaller filter inductance. The consequence of choosing a modular design will be further studied based on the analysis presented in the previous section.

As an example, Table I shows the specifications of two 3-kW AFEs which have a modular design (two 1.5-kW modules) and a one-unit design, respectively.

TABLE I
SPECIFICATIONS OF THE 3-KW AFE WITH TWO 1.5-KW MODULES AND THE 3-KW AFE WITH A 3-KW ONE-UNIT

Param.	Description	One-unit	Modular
f_1	Grid frequency	50 Hz	
E_g	Phase voltage (RMS)	110 V	
U_{dc}	DC-link voltage	385 V	
L	Filter inductance	2.5 mH	1.25 mH
f_{sw}	switching frequency	5.6 kHz	20 kHz
C_d	AFE output capacitance	1.67 mF	0.83 mF
$f_{c,PLL}$	PLL cutoff frequency	30 Hz	
δ_{PLL}	PLL damping ratio	1	
$f_{c,CL}$	CL cutoff frequency	400 Hz	800 Hz
δ_{CL}	CL damping ratio	1	
$f_{c,VL}$	VL cutoff frequency	10 Hz	40 Hz
$\delta_{c,VL}$	VL damping ratio	1	
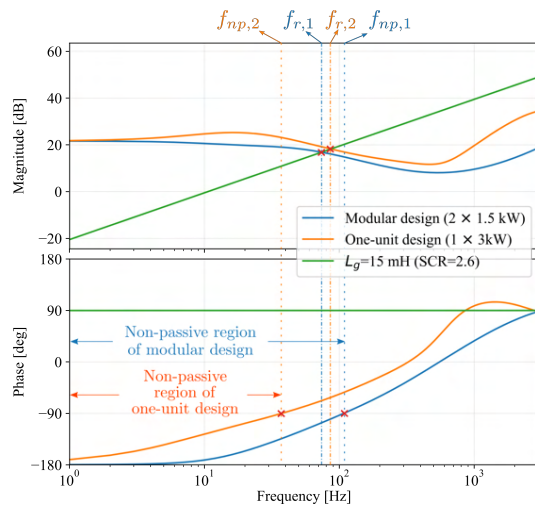
Fig. 11. Bode plots of the $Z_{dd}(s)$ of the AFE with the modular design and the one-unit design at the nominal power, i.e., 3 kW.

The bode plots of the $Z_{dd}(s)$ of the AFEs with the two designs are illustrated in Fig. 11. Clearly, the AFE with the modular design has a broader non-passive frequency range

and a smaller magnitude than the one with the one-unit design. Thus, when connecting to the same grid, the resonant frequency, namely $f_{r,1}$, of the system with the modular design based AFE is smaller than the other one $f_{r,2}$. Since the $f_{r,1}$ is within the non-passive frequency range whereas the $f_{r,2}$ is outside the non-passive region, the system with the modular design based AFE is unstable whereas the other one is stable.
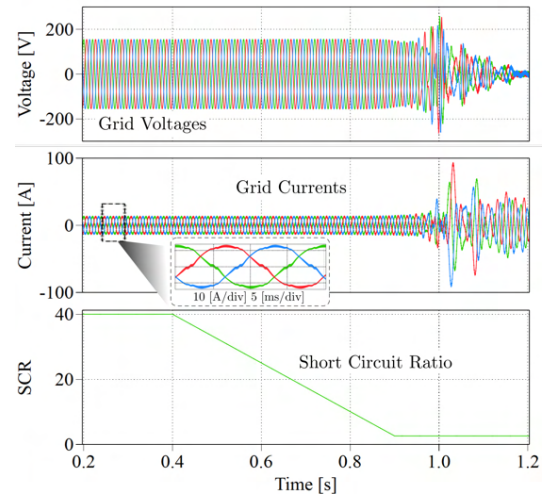
(a)
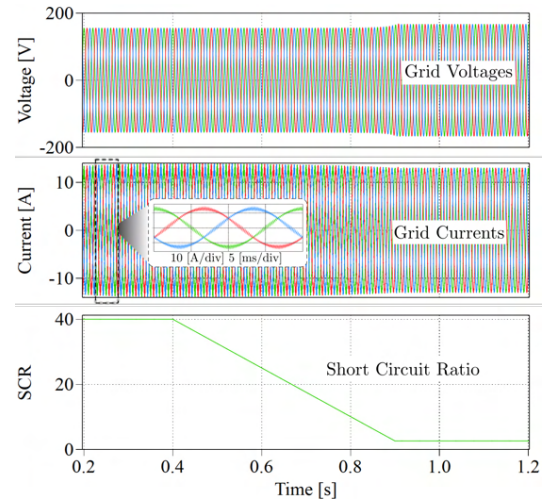
(b)

Fig. 12. Simulation verifies that the AFE with the modular design is stable in the strong grid condition but unstable in the weak grid condition while the counterpart with the one-unit design is stable in both.

Time domain simulations are carried out to verify the impedance-based analysis. Fig. 12 shows the simulation results which comply with the frequency domain analysis. As seen, the AFE with the modular design is stable when the grid is strong, i.e., SCR is 40. However, when SCR decreases to 2.6, the stability of the system is lost. A similar simulation is carried out for an AFE with the one-unit design. The results indicate that the AFE with the one-unit design is able to

1235

properly operate in both the strong grid condition and the weak grid condition.

Experiments are carried out to verify the impedance-based analysis and the simulation results. The experiment setup is shown in Fig. 13. A grid emulator is used to establish the three-phase grid voltage. Three 15-mH inductors are used to emulate the grid impedance creating a weak grid connection situation. The AFE inside an EV charger is mimicked by the Imperix power test bench. Following the AFE, two DC sources are connected to emulate the load.
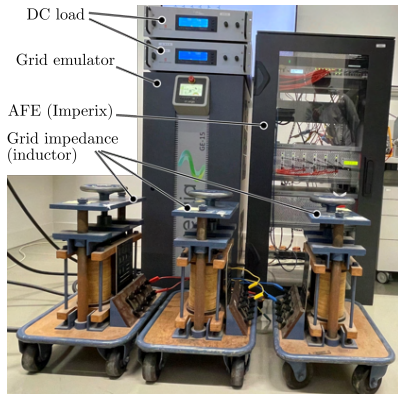
Fig. 13. Setup of the experiment.

The experiment results are shown in Fig. 14. As seen, when the grid is stiff, the systems with both two AFEs are stable, which is shown in Fig. 14a and Fig. 14b. However, when the grid inductance is high, only the one-unit design based AFE functions properly, as shown in Fig. 14c. The other one is unstable, and thereby the waveform are not shown. The experiments results are the same as the simulation results and analytical study.

Based on the analytical study and the simulation and experiment results, it can be seen that a charger with one-unit design is more suitable in a weak grid connection scenario. The reason is twofold. First, in a modular design, a higher VL cutoff frequency and a lower filter inductance are tend to be used than those in a one-unit design, which decreases the stability margin, i.e., the gap between the resonant frequency and the maximum frequency of the non-passive region. Second, since the power modules are connected in parallel, the magnitude $|Z_{dd}(s)|$ is further decreased, which reduces the stability margin one step further.

V. CONCLUSION

The paper presents how to design an EV charger's AFE to enhance the stability of the charging system with a weak grid connection. The influences of the control loop and power filter design on a charger's input impedance are studied in details. On top of that, recommendations on how to tune the controller and how to select the power filter inductance are given. Moreover, a case study comparing the stability performance of a modular design based AFE and a one-unit design based AFE is presented, which shows that using a
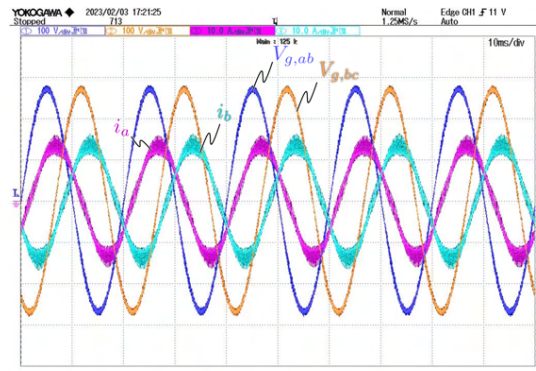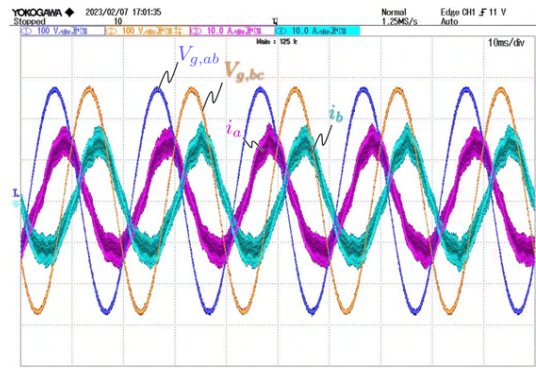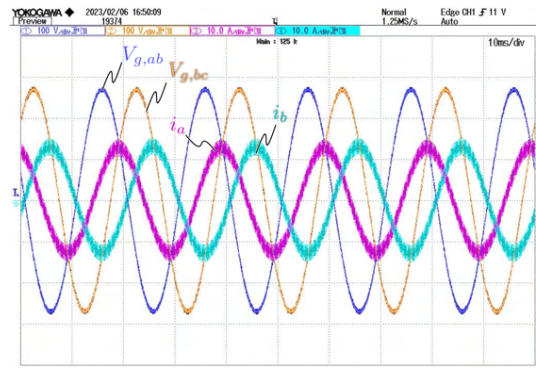
Fig. 14. Experiment results verifies the impedance-based stability analysis and the simulation. (a) and (b) show that the two AFEs are stable when the grid impedance is zero; (c) shows that the AFE with the one-unit design is still stable when the grid inductance is 15 mH (SCR=2.57).

one-unit design is more suitable in a weak grid connection scenario.

REFERENCES

[1] L. Wang, Z. Qin, T. Slangen, P. Bauer, and T. van Wijk, "Grid impact of electric vehicle fast charging stations: Trends, standards, issues and mitigation measures - an overview," *IEEE Open J. Power Electron.*, vol. 2, pp. 56–74, 2021.

[2] A. Ahmad, Z. Qin, T. Wijekoon, and P. Bauer, "An overview on medium voltage grid integration of ultra-fast charging stations: Current status and future trends," *IEEE Open Journal of the Industrial Electronics Society*, vol. 3, pp. 420–447, 2022.

[3] J. Xiao, L. Wang, Z. Qin, and P. Bauer, "A resilience enhanced secondary control for ac micro-grids," *IEEE Trans. Smart Grid*, DOI 10.1109/TSG.2023.3268245, pp. 1–1, 2023.

[4] J. Sun, "Impedance-based stability criterion for grid-connected inverters," *IEEE Trans. Power Electron.*, vol. 26, no. 11, pp. 3075–3078, 2011.

[5] L. B. Larumbe, Z. Qin, L. Wang, and P. Bauer, "Impedance modeling for three-phase inverters with double synchronous reference frame current controller in the presence of imbalance," *IEEE Trans. Power Electron.*, vol. 37, no. 2, pp. 1461–1475, 2022.

[6] L. B. Larumbe, Z. Qin, and P. Bauer, "Guidelines for stability analysis of the DDSRF-PLL using LTI and LTP modelling in the presence of imbalance," *IEEE Open J. Ind. Electron. Soc.*, vol. 3, pp. 339–352, 2022.

[7] Z. Qin, L. Wang, and P. Bauer, "Review on power quality issues in ev charging," in *2022 IEEE 20th International Power Electronics and Motion Control Conference (PEMC)*, pp. 360–366, 2022.

[8] J. Lei, Z. Qin, W. Li, P. Bauer, and X. He, "Stability region exploring of shunt active power filters based on output admittance modeling," *IEEE Trans. Ind. Electron.*, vol. 68, no. 12, pp. 11 696–11 706, 2021.

[9] L. Harnefors, X. Wang, A. G. Yepes, and F. Blaabjerg, "Passivity-based stability assessment of grid-connected vscs—an overview," *IEEE J. Emerg. Sel. Topics Power Electron.*, vol. 4, no. 1, pp. 116–125, 2016.

[10] J. Sun, "Input impedance analysis of single-phase pfc converters," *IEEE Trans. Power Electron.*, vol. 20, no. 2, pp. 308–314, 2005.

[11] S. Rivera, S. Kouro, S. Vazquez, S. M. Goetz, R. Lizana, and E. Romero-Cadaval, "Electric vehicle charging infrastructure: From grid to battery," *IEEE Ind. Electron. Mag.*, vol. 15, no. 2, pp. 37–51, 2021.

[12] B. Wen, R. Burgos, D. Boroyevich, P. Mattavelli, and Z. Shen, "Ac stability analysis and dq frame impedance specifications in power-electronics-based distributed power systems," *IEEE J. Emerg. Sel. Topics Power Electron.*, vol. 5, no. 4, pp. 1455–1465, 2017.

[13] Y. Wu, J. Xu, T. B. Soeiro, M. Stecca, and P. Bauer, "Optimal periodic variable switching pwm for harmonic performance enhancement in grid-connected voltage source converters," *IEEE Trans. Power Electron.*, vol. 37, no. 6, pp. 7247–7262, 2022.

[14] J. Xu, T. B. Soeiro, Y. Wang, F. Gao, H. Tang, and P. Bauer, "A hybrid modulation featuring two-phase clamped discontinuous pwm and zero voltage switching for 99% efficient dc-type ev charger," *IEEE Trans. Veh. Tech.*, vol. 71, no. 2, pp. 1454–1465, 2022.

[15] B. Wen, D. Dong, D. Boroyevich, R. Burgos, P. Mattavelli, and Z. Shen, "Impedance-based analysis of grid-synchronization stability for three-phase paralleled converters," *IEEE Trans. Power Electron.*, vol. 31, no. 1, pp. 26–38, 2016.

[16] R. Burgos, D. Boroyevich, F. Wang, K. Karimi, and G. Francis, "On the ac stability of high power factor three-phase rectifiers," in *2010 IEEE Energy Conversion Congress and Exposition*, pp. 2047–2054, 2010.

[17] L. Wang, Z. Qin, L. B. Larumbe, and P. Bauer, "Python supervised co-simulation for a day-long harmonic evaluation of ev charging," *Chinese J. Elect. Eng.*, vol. 7, no. 4, pp. 15–24, 2021.

[18] L. Wang, Z. Qin, and P. Bauer, "A gradient-descent optimization assisted gray-box impedance modeling of ev chargers," *IEEE Trans. Power Electron.*, vol. 38, no. 7, pp. 8866–8879, 2023.